Meteorol. Z. (Contrib. Atm. Sci.), Vol. **29**, No. 6, 493–500 (published online July 21, 2020)

Short Contributions

Numerical simulation of meteorological hazards on motorway bridges

Günter Gross*

Institut für Meteorologie und Klimatologie, Universität Hannover, Germany

(Manuscript received April 30, 2020; in revised form July 1, 2020; accepted July 1, 2020)

Abstract

A one-dimensional boundary layer model was combined with a routine to calculate surface temperatures on road bridges. Forced by reanalysis data for the year 2016, simulations were performed for two bridges 80 and 130 m in height, respectively. The results for each hour of the year were compared with on-site observations. In addition to the annual variation in general, temperature extremes captured by the model were quite reasonable. Although hourly wind speeds above the bridge were calculated less perfectly, the few cases of simulated and observed maximum mean winds were in good agreement.

Keywords: boundary layer model, bridge, road surface temperature, wind on bridges

1 Introduction

Bridges are vulnerable infrastructures exposed to the atmosphere. The highest bridges can be found in China – Beipanjiang and Yesanguan bridges with maximum heights above ground of 560 m and 470 m, respectively. In Germany, the Kochertalbrücke bridge has a clearance height of 185 m and the recently opened Hochmoselbrücke bridge is 158 m high. Each bridge reaches remarkable heights, but each one is located in completely different meteorological environments than surface roads.

Weather plays an important role in highway meteorology with respect to issues related to driver safety, deterioration of highway infrastructure, and operation and maintenance needs (Perry and Symons, 2003). These aspects are likely to become more important in the future as climate changes (Nasr et al., 2020; Willway et al., 2008).

Different meteorological variables are related to specific weather hazards on roads and bridges. In wintertime, with surface temperatures below freezing, road traffic is affected by hoar frost and ice. Dangerous situations can be found along the motorway in the form of intermittent freeze-thaw conditions. These dangers can be reduced by salting or de-icing with spray units (Feldmann et al., 2011), but these methods involve considerable expenditures on manpower, equipment, and resources to maintain the highway in safe condition.

During summertime, extreme high temperatures and long heatwaves result in thermal loading on pavement. Roadways become vulnerable due to softening and traffic-related ruts at surface temperatures even less than 50 °C (Beecroft et al., 2019). This situation increases the risk of accidents and leads to expensive projects to maintain the infrastructure. Several authors have developed techniques to estimate surface temperatures on roads and bridges by using synoptic or climatological surface observations. These data are used to calculate the temperature loads of bridge structures (e.g., Fouad, 1998; Lichte, 2004) or forecast short-term weather and road surface conditions (e.g., Raatz, 1996; Jacobs and Raatz, 1996; Kangas et al., 2015). Wistuba and Walther (2013) used the output of a regional climate model to force their road temperature model for a period of 30 years.

In the lower part of the atmosphere, wind speed increases with height. Therefore, on a bridge several hundred metres high, wind exposure of a vehicle on a bridge is greater than when moving on a surface road. In addition to mean wind speed, sharp fluctuations in speed pose a problem for vehicle stability (Kim et al., 2016). Wind shelters may reduce the risk but increase the force of the wind on the superstructure of a long-span bridge.

In this study, a one-dimensional single column boundary layer model was combined with a bridge model to calculate road surface temperatures and wind above the bridge. Forced by the results of reanalysis data, this model system was used to estimate selected meteorological hazards, as discussed above, on bridges of different heights (80 m and 130 m) for one year. Observations of the road weather information system, SWIS, of the German Meteorological Service were used to verify the model results because such a tested tool can be used to estimate potential operational failures during a bridge's lifetime.

2 The model system

The concept behind the modelling strategy was based on a combination between a simple meteorological model

*Corresponding author: Günter Gross, Institut für Meteorologie und Klimatologie, Universität Hannover, Herrenhäuser Str. 2, 30419 Hannover, Germany, e-mail: gross@muk.uni-hannover.de

DOI 10.1127/metz/2020/1040
Gebrüder Borntraeger Science Publishers, Stuttgart, www.borntraeger-cramer.com

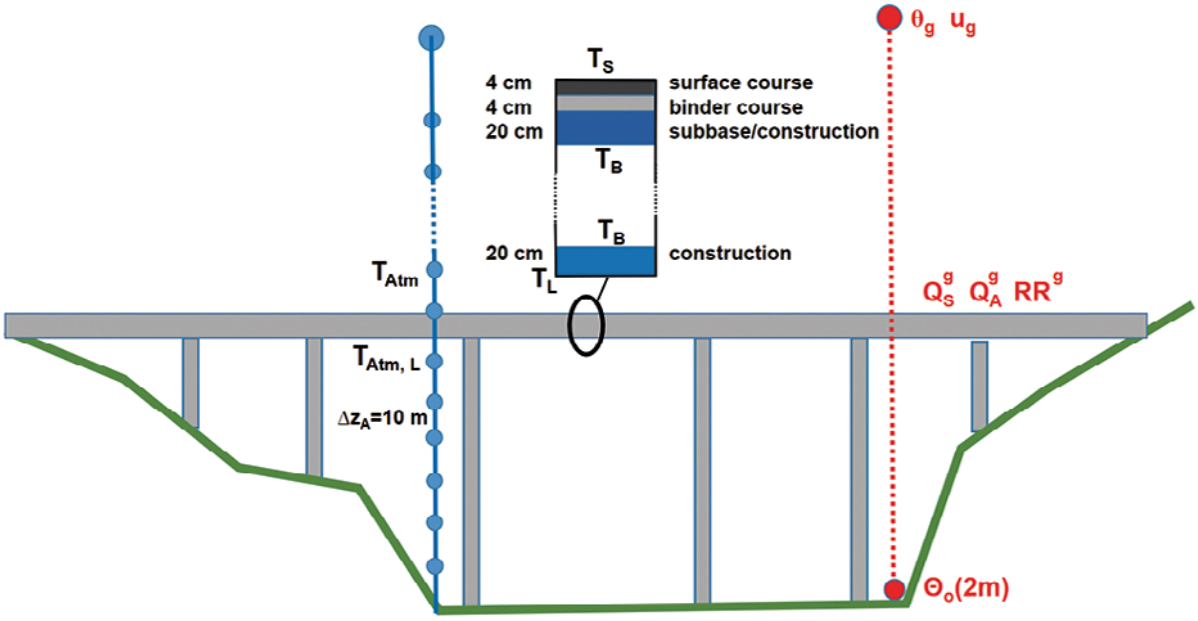

Figure 1: Schematic view of the bridge structure, nomenclature and reanalysis data used (in red).

and an embedded model to calculate temperature distribution within a bridge (Fig. 1). The one-dimensional boundary layer model (PBL model) was forced by reanalysis data to provide information on the meteorological environment of a bridge located at an arbitrary height. This weather information together with the specific structure of the bridge were used to calculate relevant long-term information, like pavement temperatures, to estimate selected hazards. This model concept is not suitable to calculate the three-dimensional distribution of wind speed and temperature around a bridge. However, if a high bridge spans a wide valley, then away from abutments at the beginning and the end of the bridge, i.e. mid-way through construction, the results should be reasonably horizontal homogeneous and therefore representative of real conditions.

2.1 The PBL model

In order to study longer periods for different synoptic situations or climate scenarios, a one-dimension single column time-dependent boundary layer model was used (Gross, 2012; Gross, 2019). It consisted of prognostic equations for the two horizontal wind components u and v, the first law of thermodynamics written with potential temperature θ, and an equation for turbulence kinetic energy E. All turbulent fluxes were parameterised using K-theory:

$$\frac{\partial u}{\partial t} = f(v - v_g) + \frac{\partial}{\partial z} K_m \frac{\partial u}{\partial z} + \frac{\partial u_g}{\partial t} \tag{2.1}$$

$$\frac{\partial v}{\partial t} = -f(u - u_g) + \frac{\partial}{\partial z} K_m \frac{\partial v}{\partial z} + \frac{\partial v_g}{\partial t} \tag{2.2}$$

$$\frac{\partial \theta}{\partial t} = \frac{\partial}{\partial z} K_h \frac{\partial \theta}{\partial z} + \frac{\partial \theta_g}{\partial t} \tag{2.3}$$

$$\frac{\partial E}{\partial t} = \frac{\partial}{\partial z} K_m \frac{\partial E}{\partial z} + K_m \left[\left(\frac{\partial u}{\partial z} \right)^2 + \left(\frac{\partial v}{\partial z} \right)^2 \right] - K_h \frac{g}{\theta} \frac{\partial \theta}{\partial z} - \frac{E^{3/2}}{l} \tag{2.4}$$

$$l_a = \frac{\kappa z}{1 + \kappa z / l_\infty}, \quad l_\infty = 25\,\mathrm{m}, \quad \kappa = 0.40 \tag{2.5}$$

$$K_m = a l_a \sqrt{E}, \quad a = 0.2 \tag{2.6}$$

where u and v are wind components in west-east and south-north directions, u_g and v_g are components of the larger scale synoptic wind, f is the Coriolis parameter, θ is the potential temperature, θ_g is the synoptic temperature, l_a is the mixing length, K_m and K_h are eddy diffusivities for momentum and heat ($K_m = K_h = K$ are used here) and g is acceleration due to gravity.

The effects of thermal stability on turbulent mixing in the boundary layer were considered by a stratification dependent mixing length:

$$l = l_a / \Phi \tag{2.7}$$

where Φ represents the local universal function which may, according to Wippermann (1973), be expressed as:

$$\Phi = (1 - 15 z/L)^{-1/4}, \qquad z/L \le 0 \quad \text{or}$$
$$\Phi = 1 + 4.7 z/L, \qquad z/L > 0 \tag{2.8}$$

where L denotes the Monin-Obukhov stability length.

The synoptic forcing u_g, v_g, and θ_g and the boundary conditions were adopted from the high-resolution reanalysis system (Bollmeyer et al., 2015). The regional reanalysis data for the European CORDEX EUR-11 domain are available at a 6 km grid resolution. These values were also used as boundary conditions at the upper boundary, updated every hour, and linearly interpolated

Table 1: Contributions to the surface energy budget on the top and the bottom side of a bridge.

	Bridge surface T_S	**Bridge underside T_L**
Q_{SB}	$(1-a_B)Q_S^g$ (Q_S^g from reanalysis data)	not considered
Q_L	$\varepsilon_B \sigma T_S^4$	$\varepsilon_B \sigma T_L^4$
Q_A^g	from the atmosphere (from reanalysis data)	from the ground under the bridge $\varepsilon_o \sigma T_o^4$
Q_H	$c_p \rho K \frac{\partial T}{\partial z} = c_p \rho K \frac{T_{\mathrm{Atm}} - T_V}{\Delta z_A}$	$c_p \rho K \frac{\partial T}{\partial z} = c_p \rho K \frac{T_{\mathrm{Atm},L} - T_L}{\Delta z_A}$
Q_V	function of precipitation RR^g and Q_S^g	not considered
Q_B	$\lambda \frac{\partial T}{\partial z} = \lambda \frac{T_B - T_S}{\Delta z_B}$	$\lambda \frac{\partial T}{\partial z} = \lambda \frac{T_B - T_L}{\Delta z_B}$

in between. At the lower boundary, 2 m temperatures from reanalysis data were used, while zero wind conditions were adopted as well as turbulence kinetic energy proportional to the simulated friction velocity squared.

The equations were integrated forward in time on 70 grid levels in the atmosphere with a time step of $\Delta t = 60$ s. The grid resolution was 10 m up to a height of 400 m, followed by continuous expansion up to the model height of 2000 m.

2.2 The bridge model

The bridge structure used in this study was a long-span box girder bridge made of steel or reinforced concrete. The bridge deck was covered with an asphalt surface course and a binder course, together 8 cm thick, which were applied to the subbase and the bridge construction (Fig. 1). The lower part of the girder consisted of a solid construction of 20 cm thickness.

As summarized in Table 1, temperatures at the bridge surface T_S and the underside of the bridge T_L were derived by a surface energy budget which included shortwave radiation balance Q_{SB}, longwave radiation Q_L, longwave radiation from above or below Q_A, turbulent fluxes of sensible and latent heat Q_H and Q_V, and heat transfer into the underlying structure Q_B (e.g., Stull, 1988). A positive sign is used for an energy gain, a negative sign for energy loss of the surface.

In the equations above, a_B is albedo, ε is emissivity (ε_B for the bridge and ε_o for the surface beneath the bridge), c_p is specific heat, ρ is air density, T_{Atm} is simulated temperature at nearest grid level in the atmosphere above and $T_{\mathrm{Atm},L}$ below the bridge at distance $\Delta z_A = 10$ m, λ is thermal conductivity, and T_B is the simulated internal temperature of the bridge at distance $\Delta z_B = 2$ cm.

Evaporation is an important factor which determines the surface temperature T_S. When the road surface is dry ($Q_V = 0$), a large portion of the direct solar radiation is used for heating the road's surface. When water is available on the road (e.g., after precipitation), a rough estimate of $Q_V = 0.3\, Q_{SB}$ was used to calculate the turbulent latent heat flux. Although this is a crude assumption which might fail some days, the effects on the hazard 'high pavement temperature' was low because extreme values of T_S occurred during sunny days.

To calculate the lower boundary for air temperature above the bridge, an additional thin microlayer in which molecular processes dominate was included at the interface between the smooth road surface and the atmosphere. Assuming that the molecular heat flux at the surface is equal to the turbulent heat flux at the top of the microlayer (Stull, 1988), the air temperature T_V at the top of the viscous layer above the bridge can be calculated as:

$$T_V = \frac{T_S + cT_{\mathrm{Atm}}}{1 + c} \tag{2.9}$$

with $c = \frac{K \Delta z_V}{\nu_L \Delta z_A}$ and $\nu_L = 1.5 \times 10^{-5}$ m^2/s for air and a viscous layer depth of $\Delta z_V = 1$ mm.

The height of the rainwater h (in mm) on the surface was calculated according to:

$$h^{t+\Delta t} = h^t - \frac{Q_V}{L} \Delta t + RR^g \Delta t \tag{2.10}$$

with latent heat L and precipitation RR^g (mm/s). The range of h is limited to $h = 0$ (dry surface, $Q_V = 0$) and $h = 2$ mm. For larger values of h, surface run off removes the excess water.

For temperatures inside the bridge material T_B, the heat conduction equation is:

$$\frac{\partial T_B}{\partial t} = \upsilon_B \frac{\partial^2 T_B}{\partial z_B^2} \tag{2.11}$$

with thermal diffusivity ν_B. Depending on the inner structure of the bridge, different values for ν_B were specified for each layer.

Based on data published by Fouad (1998) and Lichte (2004), the properties of the asphalt surface layer were fixed with $a_B = 0.2$, $\varepsilon_B = 0.9$, $\nu_B = 0.4 \times 10^{-6}$ m^2/s and $\lambda = 0.8$ W/m/K. For steel and reinforced concrete, values of $\nu_B = 13 \times 10^{-6}$ m^2/s and $\nu_B = 0.7 \times 10^{-6}$ m^2/s were used, respectively. The emissivity of the ground under the bridge was fixed with a value of $\varepsilon_o = 0.95$.

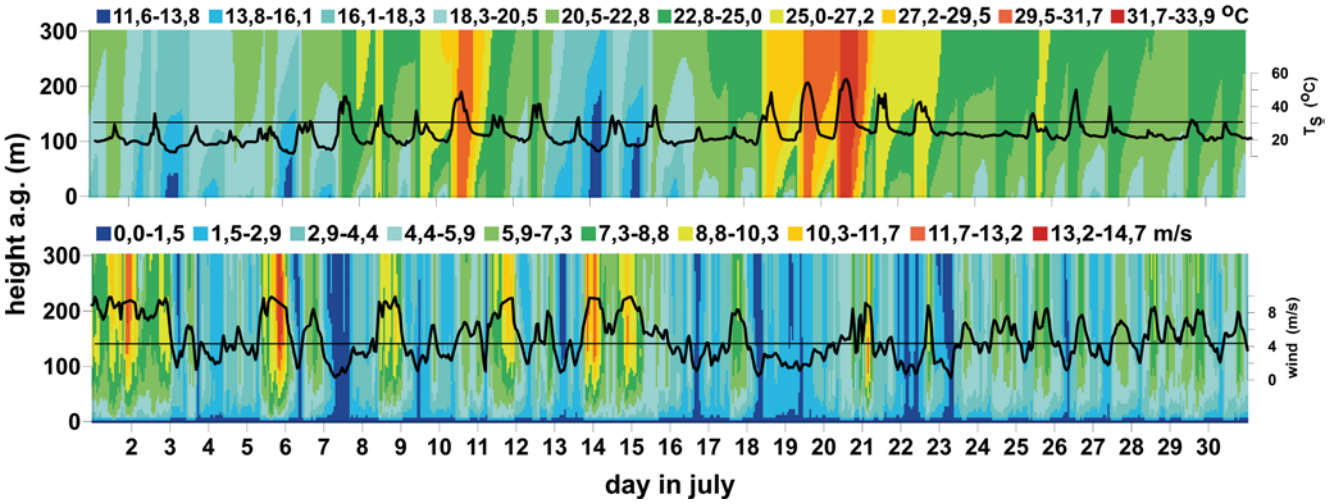

Figure 2: Time-height cross section for July 2016 of simulated temperature (above) and wind speed (below) at site K266 on Moseltalbrücke. Surface temperature T_S on the 130 m high bridge and wind speed at 2 m height above the bridge are enclosed in solid lines.

The temperature distribution inside the girder bridge was calculated at 70 levels with a time step of $\Delta t = 60$ s; at the top and bottom, the grid resolution was 2 cm with values increasing towards the inner part.

3 Observations and synoptic forcing

The German National Meteorological Service (DWD) collect and provides information about the surface status and meteorological conditions close to roads at specific sites (Glättemeldeanlagen GMAs). Every 15 minutes, wetness and temperature of the pavement T_S^{obs} are recorded as well as atmospheric temperature $T_{2\,m}^{\text{obs}}$ and wind speed as a 10-min mean along the roadside. Air temperature and wind are measured as standard at a height of 2 m and surface temperature is observed at the outermost fast lane. Data from the year 2016 for two GMAs located on high bridges were selected (Koelschtzky, 2018, personell communication) to compare with the model. The Moseltalbrücke bridge (GMA K266), located to the west of Koblenz, is a 936 m long-span steel bridge with a superstructure height of around 6 m and a maximum height of the roadways above ground of 136 m. Data availability for the year 2016 was 98.5 %. For synoptic forcing, reanalysis of data in 1 hour intervals at a grid point with coordinates (longitude/latitude) 50.359 N/7.498 E were used; however, precipitation was not available with a 1 hour resolution, therefore data from the nearby synoptic station Andernach (ID 0161) were used. For an additional application, the 845 m long Haseltalbrücke bridge (GMA M731) near Suhl was chosen. The maximum height above ground of this girder bridge with a superstructure height of 5 m is 80 m. Data availability was 95–99 % for meteorological parameters at the roadside and 90 % for road surface temperatures. Reanalysis data from a grid point with coordinates 50.603 N/10.674 E and hourly precipitation data from the synoptic station Erfurt-Weimar (ID 1270) were used to specify the synoptic forcing.

4 Results

Numerical simulations with the model system were performed for the full year 2016 for both bridges, whereby results for the higher Moseltalbrücke will be discussed first and in more details. Wind speed and temperature for the month July are shown as time-height cross sections in Fig. 2. A well-developed diurnal variation for temperature is evident with low nocturnal temperatures near the surface and an inversion layer above. On some days, atmospheric near surface temperatures are above 30 °C within a well-mixed boundary layer during daytime. Wind speeds show periodic variations over time, with high values usually during the daytime. Only a few nights (e.g., July 14–15), did strong nocturnal winds occur which might be due to a low-level jet.

Simulated temperatures on the road surface at a height of 130 m above ground are also included in Fig. 2. During the sunny period (July 19–21), maximum temperatures T_S were above 50 °C. One hour mean wind speeds at a height of 2 m above the bridge deck, the usual measuring height of a GMA, were calculated using a log-linear law with simulated wind speeds at 10 m above the bridge and a surface roughness length of 1 cm. These values, at a height of approximately 130 m above ground, are also included in Fig. 2 and show strong variations with maximum values up to 8 m/s. Using the temperature T_V near the surface and the temperature 10 m above the bridge T_{Atm}, a 2 m air temperature was calculated in the same way.

In Fig. 3, a comparison between the simulated and the observed minimum and maximum surface temperatures and the 2 m temperatures is presented. The observations at GMA K266 on the 130 m high Moseltalbrücke bridge show maximum surface temperatures that frequently exceed 40 °C between day 120 and day 250. Minimum surface temperatures were regularly below freezing between days 1 and 120 and days 310 to 366.

The main features of the annual course of simulated temperatures are in close agreement with the observa-

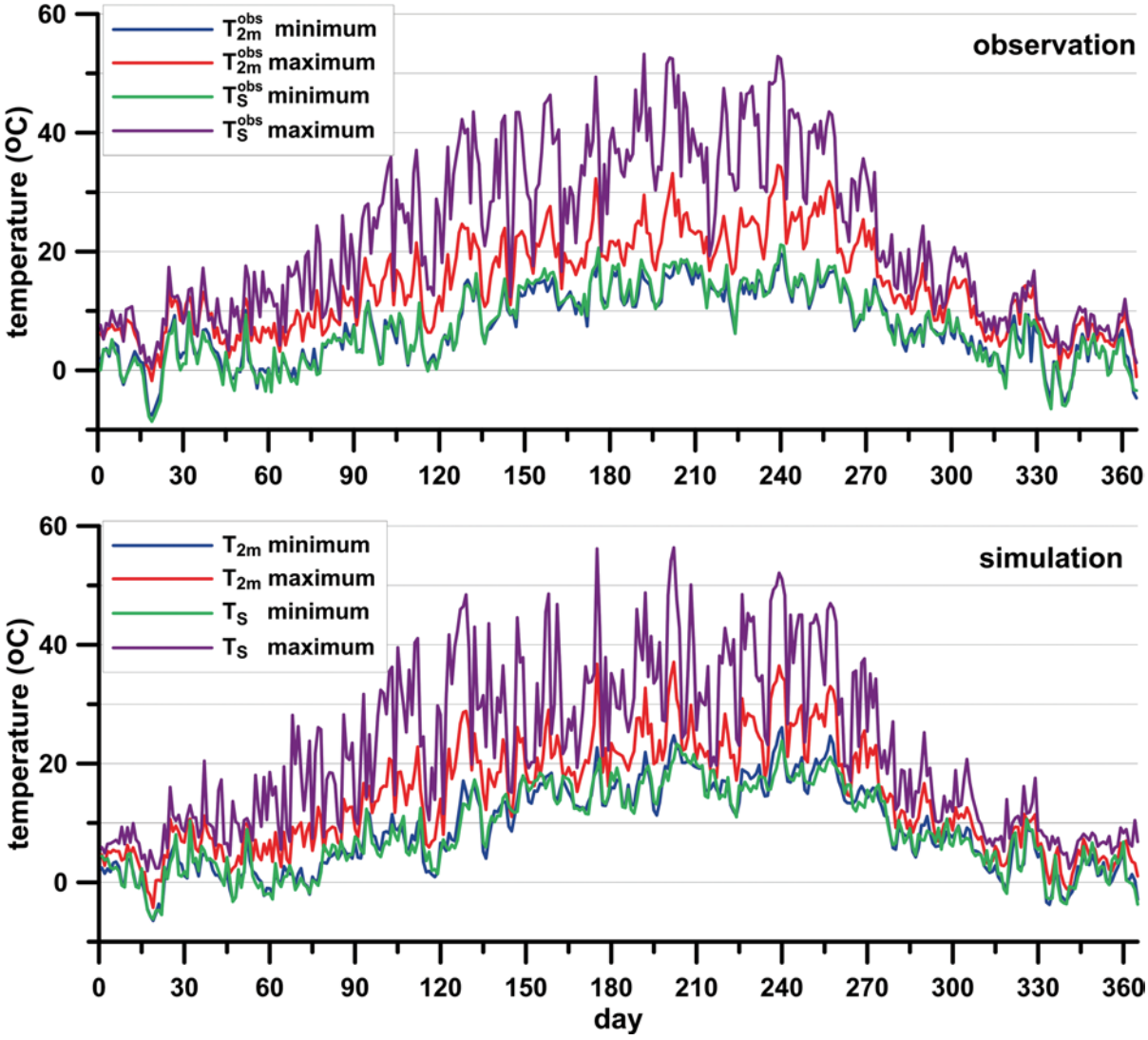

Figure 3: Observed (above) and simulated (below) annual variation of daily minimum and maximum temperatures of road surface and at 2 m height above the road at site K266 on Moseltalbrücke.

tions. Only during the summer months were minimum road surface temperatures and nocturnal 2 m air temperatures higher than the observed values. This agreement is also evidenced by direct comparison (Fig. 4). Daily maximum road surface temperatures and night-time minimum road surface temperatures were simulated in the same order as the observed values. A statistical evaluation of mean absolute difference MAD and coefficient of determination R^2 results in MAD = 1.7 K und $R^2 = 0.93$ for the night-time situation and MAD = 3.3 K and $R^2 = 0.88$ for daytime respectively. Simulated and observed maximum temperatures for some days were well above 50 °C, while simulated road surface temperatures were below freezing on 55 days compared to an observed number of 61 days. Beside these mean surface temperature extremes, daily range between maximum and minimum temperatures were compared (Fig. 5). The same analysis was performed for the 2 m air temperature above the bridge, estimated by a log-linear law. Although amplitudes showed large values, simulated results capture the overall picture of the observations quite well.

High wind speeds and strong gusts can increase the danger to vehicles crossing a wind-exposed infrastructure such as a high bridge. In addition to strong day-to-day variations, the synoptic conditions at the selected sites caused higher values of mean wind speed during winter and lower values during the summer months. In Fig. 6, the observed maximum 1 hour mean wind speed for each day of the year 2016 at Moseltalbrücke is given together with the simulated wind speed. The numerical results follow the observations closely which is additional evidence for comparison (Fig. 6). Although there is some scatter, the simulation captures the range of the observed wind speed (MAD = 1.4 m/s and $R^2 = 0.56$).

Depending on traffic, speed, size, and load of motor vehicles, wind speed might pose a danger for vehicles crossing a long high bridge. Kim et al. (2016) estimated

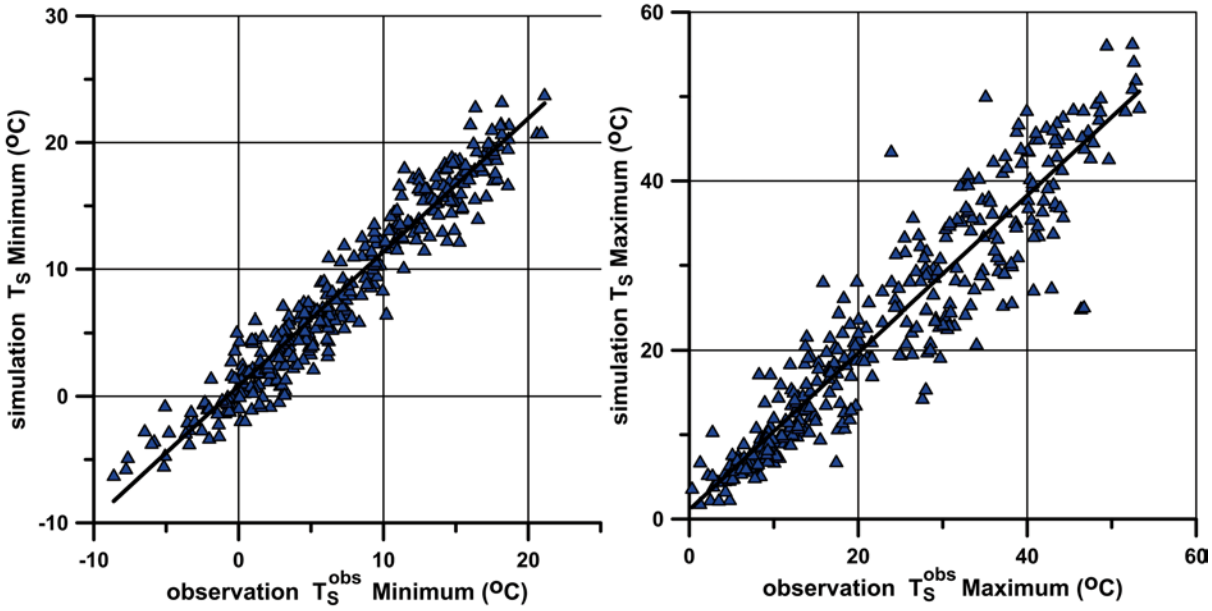

Figure 4: Simulated and observed daily minimum (left) and maximum (right) surface temperatures at site K266 on Moseltalbrücke.

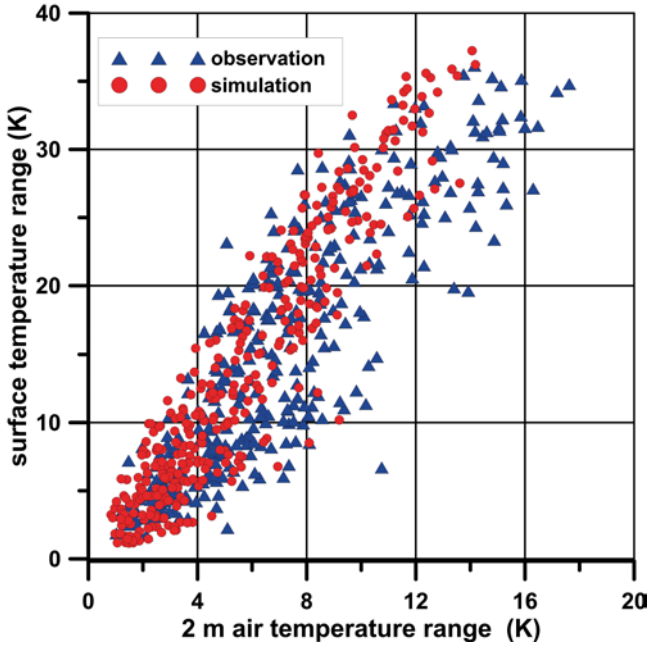

Figure 5: Simulated and observed diurnal ranges of the road surface temperature and the air temperature at 2 m height above the road at site K266 on Moseltalbrücke.

critical wind speeds at a Beaufort scale of Bf 8 to Bf 9 (approximately 17–24 m/s) for sideslip and overturning of motor vehicles. High wind speeds may occur as a generally high mean wind speed U or as a sudden and unforeseen gust event u_{gust}. Gusts are not measured at the GMA but may be estimated by the calculated wind speed and turbulence information generated by the model. An approach commonly used in practice is given by:

$$u_{\text{gust}} = U + f_g \sigma_u \tag{4.1}$$

Table 2: Comparison of observed and simulated frequency of selected meteorological caused hazards at the Moseltalbrücke (K266) and the Haseltalbrücke (M731) for the year 2016.

	observation		simulation			
	K266	M731	K266	M731	K266	M731
days with U > Bf 7	3	0	2	1	u_{gust}: 16	27
days with U > Bf 8	0	0	0	0	u_{gust}: 2	2
hours T_S < 0 °C	420	859	363	753		
freeze-thaw change	86	125	97	190		
hours T_S > 40 °C	232	108	214	102		
hours T_S > 45 °C	84	31	86	30		
hours T_S > 50 °C	20	4	20	6		

where σ_u is the standard deviation of wind speed calculated via the turbulence kinetic energy, and the factor f_g is typically on the order of three (Koss, 2006).

Meteorological hazards due to temperature in wintertime are situations with temperatures below zero and changes in freeze-thaw conditions. In summertime, high surface temperatures may cause severe damage to the road surface and the substructure. In Table 2, these hazards are summarised for the Moseltalbrücke and Haseltalbrücke sites for the year 2016 for the observations and the simulation.

The numerical results are close to the observations and thus demonstrate that the model combination from reanalysis data down to the bridge model is an encouraging procedure to estimate in situ meteorological conditions. As observed at GMA K266 and in the simulation results, the 10-min mean wind speed on the bridge did not reach gale force; however, in the simulation, wind gusts occurred on several days with short time peak winds exceeding Bf 8.

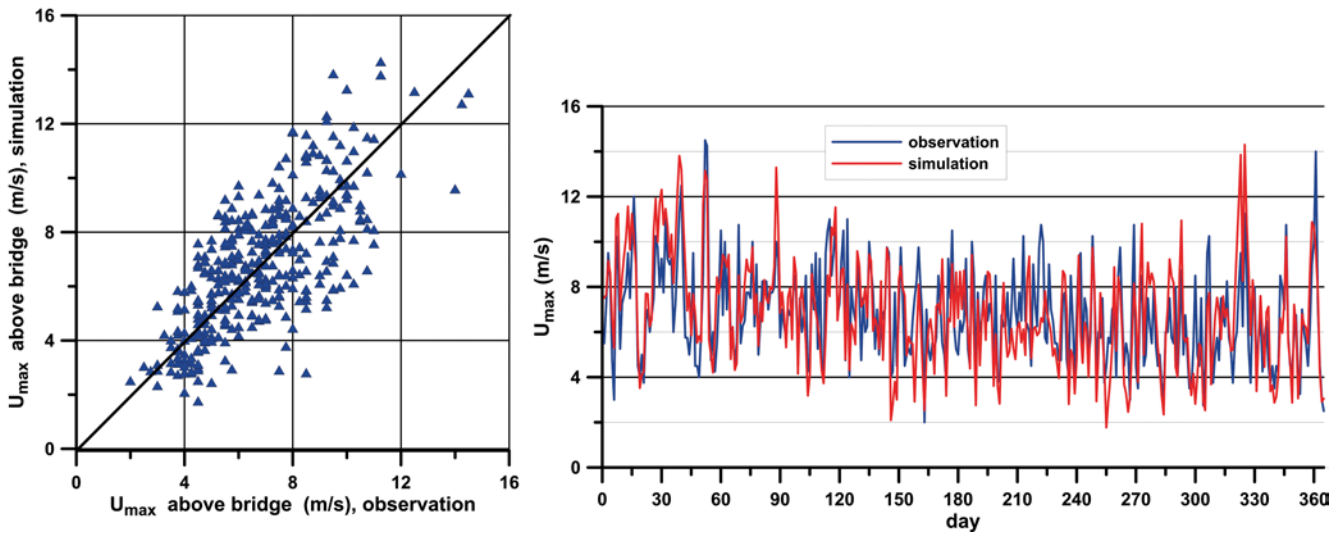

Figure 6: Annual variation of daily maximum mean wind speed at 2 m above the bridge at site K266 on Moseltalbrücke (right). Comparison of observed and simulated 2 m daily mean wind speed maximum (left).

The number of hours below freezing were underestimated by the model, while a large number of freeze-thaw changes were simulated. However, the numbers were on the same order of magnitude and differences of 10–15 % are reasonable against the background of uncertainties in observations and model results. On the other hand, surface temperatures above 40 °C were captured well by the model, especially extreme temperatures.

Numerical simulations were performed also for the M731 site at Haseltalbrücke in order to test the applicability of the model in an alternative situation. The procedure was the same as for the Moseltalbrücke bridge. The quality of the results was similar, so only the comparison of the selected meteorological hazards is given in Table 2.

Wind speed, in general, was lower near M731 (annual mean 2.1 m/s) compared to K266 (annual mean 3.9 m/s) due to climatological conditions and lower bridge height. Mean wind speeds above Bf 6 were rare in the observations and in the simulation; however, closer to the ground, the turbulence was greater (Stull, 1988), and consequently, the number of simulated wind gusts calculated by Equation (4.1) were greater as well.

Temperatures below zero degrees at the Haseltalbrücke location were more frequent than at the Moseltalbrücke location mainly because of the general climatological situation. Night-time minimum air temperatures during the winter season are typically two degrees lower at M731 on the Haseltalbrücke than at K266 located on the Moseltalbrücke. In combination with lower wind speed, this is the reason that the number of hours below freezing, as well as the number of freeze-thaw cycles, which were much higher at Haseltalbrücke than at Moseltalbrücke. Again, the model system reproduced the order of events, but with larger differences compared to observed values at M731 than at K266. Again, the approach used in this study was successful in simulating the occurrence of high surface temperatures on the road at K266. Nearly all situations in the year 2016 with $T_S > 40$ °C were captured by the model. It is noteworthy that the number of high surface temperatures was much smaller at M731 than at K266. An obvious reason for this finding is the lower number of days with high values of direct solar radiation in the reanalysis data. At the Moseltalbrücke site in the summer period of 2016, Q_S exceeded 600 W/m^2 for a total of 20 days, while at Haseltalbrücke, this only occurred on seven days.

5 Conclusions

A one-dimensional boundary layer model was used to simulate the time-height variation of wind speed and temperature forced by reanalysis data from the year 2016. In this atmospheric environment, a bridge with a certain height and local atmospheric variables, together with key parameter characterising the structure of the bridge, were used to calculate surface temperatures of the pavement. In addition, atmospheric wind speed and temperature at a height of 2 m above the bridge deck were estimated. The simulation results were compared to observations for two long-span bridges of 80 m and 130 m height at two sites in Germany.

The model system introduced here is suitable to simulate the diurnal and annual variation in good agreement with the available observations. High surface temperatures, where pavement becomes vulnerable through softening, were captured for both bridges by the model. Minimum winter temperatures and freeze-thaw conditions were simulated with slightly poorer agreement, but still on the same order as observed. This is not surprising since the maximum temperature mainly depends on the magnitude of the solar radiation, while a variety of parameters like fog, cloud coverage, or surface wetness are responsible for surface temperatures a little below or above the freezing point. Observed mean wind speeds above the bridge never exceeded 15 m/s on both bridges

during the year. Also, in the simulation forced by reanalysis data, mean wind speeds never reached stormy conditions; however, estimated gusts were of an order that was a potential danger for vehicles moving across the bridge deck.

Bridge operators need information about possible meteorological hazards in order to include precautionary measures during the planning process or to estimate the operational failures during a bridge's lifetime. Although presented results are very encouraging, the models used have limitations and involve uncertainties. All three-dimensional features concerning the bridge structure or meteorological characteristics in a mountain environment like channeling of the air flow in valleys or diurnal wind systems cannot be captured by the one-dimensional approach. If the results of regional climate models for different scenarios can be used for large scale forcing, the simple model system presented her is applicable to estimate the impact of future climate change on the occurrence of specific meteorological hazards on bridges.

Acknowledgements

The author would like to thank the reviewers for their careful reading and very useful comments, which improved the quality of the paper significantly. The author would like to thank T. Lucas, Department of Meteorology and Climatology, Leibniz University Hannover for providing the reanalysis data. The publication of this article was funded by the Open Access Fund of the Leibniz Universität Hannover.

References

Beecroft, A., D. Bodin, E. van Aswegen, J. Grobler, 2019: Roads vs extreme weather: designing more resilient roads. – Infrastructure Exchange, https://www.infrastructure-exchange.com/post/roads-vs-extreme-weather-designing-more-resilient-roads.

Bollmeyer, C., J.D. Keller, C. Ohlwein, S. Bentzien, S. Crewell, P. Friederichs, A. Hense, J. Keune, S. Kneifel, I. Pscheidt, S. Redl, S. Steinke, 2015: Towards a high-resolution regional reanalysis for the European CORDEX domain. – Quart. J. Roy. Meteor. Soc. **141**, 1–15.

Feldmann, M., B. Döring, J. Hellberg, M. Kuhnhenne, D. Pak, 2011: Vermeidung von Glättebildung auf Brücken durch die Nutzung von Geothermie. – Berichte der Bundesanstalt für Straßenwesen, Heft B **87**, 77 pp.

Fouad, N.A., 1998: Rechnerische Simulation der klimatisch bedingten Temperaturbeanspruchungen von Bauwerken. – Berichte aus dem Konstruktiven Ingenieurbau, Heft **28**, TU Berlin.

Gross, G., 2012: Numerical simulation of greening effects for idealised roofs with regional climate forcing. – Meteorol. Z. **21**, 173–181.

Gross, G., 2019: On the range of boundary layer model results depending on inaccurate input data. Meteorol. Z. **28**, 225–234.

Jacobs, W., W.E. Raatz, 1996: Forecasting road-surface temperatures for different site characteristics. – Meteor. Appl. **3**, 243–256.

Kangas, M., M. Heikinheimo, M. Hippi, 2015: RoadSurf: a modelling system for predicting road weather and road surface conditions. – Meteor. Appl. **22**, 544–553.

Kim, S.E., C.-H. Yoo, H.K. Kim, 2016: Vulnerability assessment for the hazards of crosswinds when vehicles cross a bridge deck. – J. Wind Eng. Ind. Aerodyn. **156**, 62–71.

Koelschtzky, W., 2018: personal communication. – DWD Offenbach.

Koss, H.H., 2006: On the differences and similarities of applied wind comfort criteria. – J. Wind Eng. **94**, 781–797.

Lichte, U., 2004: Klimatische Temperatureinwirkungen und Kombinationsregeln bei Brückenbauwerken. – Dissertation, Universität der Bundeswehr, München.

Nasr, A., E. Kjellström, I. Björnsson, D. Honfi, O.L. Ivanov, J. Johansson, 2020: Bridges in a changing climate: a study of the potential impacts of climate change on bridges and their possible adaptations. – Structure Infrastructure Engineering **16**, 738–749.

Perry, A.H., L.J. Symons, 2003: Highway Meteorology. – Taylor & Francise-Library.

Raatz, W.E., 1996: Straßenwettervorhersage des Deutschen Wetterdienstes im Rahmen des Straßenzustands- und Wetterinformationssystems (SWIS). – promet **25**, 1–8.

Stull, R.B., 1988: An introduction to boundary layer meteorology. – Kluwer Academic, 666 pp.

Willway, T., L. Baldachin, S. Reeves, M. Harding, M. McHale, M. Nunn, 2008: The effects of climate change on carriageway and footway pavement maintenance. – Technical report PPR **184**, Dept. Transport, Berkshire, UK.

Wippermann, F., 1973: The planetary boundary layer. – Ann. Meteorol. **7**, 346 pp.

Wistuba, M.P., A.Walther, 2013: Soll der prognostizierte Klimawandel für die rechnerische Dimensionierung von Asphaltstraßen berücksichtigt werden. – Straße und Autobahn **3**, 140–147.